Nanoscale Horizons

ROYAL SOCIETY OF CHEMISTRY

COMMUNICATION

View Article Online
View Journal | View Issue

Cite this: *Nanoscale Horiz.*, 2020, 5, 971

Received 22nd December 2019,
Accepted 30th March 2020

DOI: 10.1039/c9nh00802k

rsc.li/nanoscale-horizons

Photoluminescence enhancement of MoS_2/CdSe quantum rod heterostructures induced by energy transfer and exciton–exciton annihilation suppression†

Yang Luo,[a] Hangyong Shan,[a] Xiaoqing Gao,[b] Pengfei Qi,[a] Yu Li,[a] Bowen Li,[a] Xin Rong,[a] Bo Shen,[a] Han Zhang,[a] Feng Lin,[a] Zhiyong Tang[c] and Zheyu Fang *[a]

Energy transfer in heterostructures is an essential interface interaction for extraordinary energy conversion properties, which promote promising applications in light-emitting and photovoltaic devices. However, when atomic-layered transition metal dichalcogenides (TMDCs) act as the energy acceptor because of strong Coulomb interactions, the transferred energy can be consumed by nonradiative exciton annihilations, which hampers the development of light-emitting devices. Hence, revealing the mechanism of energy transfer and the related relaxation processes from the aspect of the acceptor in the heterostructure is key to reducing nonradiative loss and optimizing luminescence. Here, we study the exciton dynamics from the standpoint of the acceptor in MoS_2/CdSe quantum rod (QR) heterostructures and realize efficiently enhanced photoluminescence (PL). Through femtosecond pump–probe measurements, it is directly observed that energy transfer from CdSe QRs largely raises the exciton population of the acceptor, MoS_2, providing a larger emission "source". In addition, the dielectric environment introduced by CdSe QRs efficiently enhances the PL by suppressing exciton–exciton annihilation (EEA). This study provides new insights for on-chip applications such as light-emitting diodes and optical conversion devices based on low dimensional semiconductor heterostructures.

New Concepts

We reveal the unique mechanism of PL enhancement in MoS_2/CdSe quantum rod (QR) heterostructures from the standpoint of the acceptor. The mechanism involves energy transfer and suppression of exciton–exciton annihilation. The physical mechanism of energy transfer has been proposed for several decades. However, how the transferred energy influences the exciton decay of the acceptor has not been addressed. In monolayered two-dimensional transition metal dichalcogenides (TMDCs), the nonradiative exciton annihilation is more intense compared to other semiconductors due to the strong reduced dimension, and thus the transferred energy can dissipate in a nonradiative way, which seriously hinders terminal luminescence efficiency. Using ultrafast pump–probe measurements, we demonstrate that the transferred energy can "re-excite" excitons in the MoS_2 acceptor and the nonradiative annihilation process can be effectively suppressed by the CdSe QRs. Additionally, the contribution of energy transfer and exciton–exciton annihilation to exciton relaxation can be modulated to improve the final photoluminescence. Our work advances the basic comprehension of the exciton dynamics of the energy acceptor and paves the way for developments in new high-performance optical conversion, on-chip light emission, and light-sensing devices.

Introduction

With the development of nanotechnology, low dimensional heterostructures have attracted vast attention due to novel effects such as energy transfer,[1,2] charge transfer,[3–5] and Moiré superlattice properties,[6] yielding potential applications in light-harvesting and photoelectron devices.[7,8] Nonradiative energy transfer in heterostructures is a process that transfers energy from a "donor" to an "acceptor" through near-field interactions to achieve energy conversion.[9,10] In particular, with atomic transition metal dichalcogenide (TMDC)/quantum confined semiconductor (quantum rods,[11] quantum dots,[12] and quantum nanoplatelets[13]) heterostructures, energy transfer can help atomic TMDCs break their light emission limit by providing extra energy from quantum rods (QRs), which can lead to high quantum yields of monolayered TMDC-based devices. In recent years, approaches such as inducing an electrical field,[14] altering the number of TMDC layers,[15] tuning the donor size of the heterostructures[16] as well as changing the polarization between the donor and acceptor[17] have been employed to modulate energy transfer in heterostructures effectively.

[a] *School of Physics, State Key Laboratory for Mesoscopic Physics, Academy for Advanced Interdisciplinary Studies, Collaborative Innovation Center of Quantum Matter, and Nano-optoelectronics Frontier Center of Ministry of Education, Peking University, Beijing 100871, P. R. China. E-mail: zhyfang@pku.edu.cn*
[b] *College of Physics and Optoelectronic Engineering, Shenzhen University, Guangdong 518060, P. R. China*
[c] *CAS Key Laboratory of Nanosystem and Hierarchical Fabrication, CAS Center for Excellence in Nanoscience, National Center for Nanoscience and Technology, Beijing 100190, P. R. China*

† Electronic supplementary information (ESI) available. See DOI: 10.1039/c9nh00802k

However, most of the above-mentioned studies are focused on the energy transfer efficiency and exciton relaxation properties from the perspective of the donor. The acceptor usually acts as the final output terminal in applications, where the transferred energy can decay by both radiative and nonradiative channels. When the thickness of the acceptor in TMDCs is reduced to the monolayer scale, nonradiative relaxation such as exciton–exciton annihilation (EEA) and high order exciton–exciton annihilation (HOEEA) become more active, which accelerates exciton consumption and the exciton lifetime decreases to tens of picoseconds.[18] Thus, a large portion of the transferred energy in the acceptor is consumed in a nonradiative way, which strongly attenuates the PL emission. In order to achieve applications in high quantum yield devices, it is urgent to study the exciton relaxation process from the perspective of acceptor and explore ways to suppress the nonradiative decay of excitons.

In this study, we investigate the exciton relaxation dynamics of MoS_2/CdSe QR heterostructures from the standpoint of the energy acceptor to reveal its unique mechanism of PL enhancement. The femtosecond pump–probe technique was employed to investigate how the transferred energy affects the exciton relaxation of MoS_2 and the effective suppression of the nonradiative decay. This study provides a new physical understanding of the exciton dynamics of low dimensional heterostructures and lays the foundation for highly efficient solar cells, ultralow-threshold lasers, light-emitting diodes, and sensitive optical detectors.

Results and discussion

In the heterostructure, CdSe QRs with L-cysteine ligands are distributed on a MoS_2 monolayer (Fig. 1(a)). Excitons of MoS_2 and CdSe QRs are pumped using 400 nm laser excitation. The reduced Coulomb screening of the MoS_2 monolayer enables multi-exciton interactions such as HOEEA and EEA occur in a very short time. The energy band structures of the MoS_2 monolayer, CdSe QRs, and L-cysteine molecules are shown in the inset, and the corresponding band values have been reported in previous studies.[19–21] As the energy of the excitation photon is around 3.05 eV, which is lower than the excitation energy of L-cysteine, only excitons in CdSe and MoS_2 are excited and a high energy barrier is formed by the L-cysteine molecules. In addition, L-cysteine is an amino acid with high resistance that can suppress interfacial charge transfer even in a single layer.[22] Thus, the effects of charge transfer between CdSe QRs and MoS_2 are very weak, and the dominating interaction between CdSe QRs and the MoS_2 monolayer is energy transfer through near-field coupling. Processes such as energy transfer, EEA, and HOEEA affect the final light emission of the MoS_2 monolayer. To obtain the morphology of the heterostructure, reflection mapping was performed (Fig. 1(b)). The homogeneous blue area indicates that CdSe QRs are distributed almost uniformly on the top of the MoS_2 monolayer, which indicates that optical effects induced by the aggregation of QRs are trivial (AFM mapping

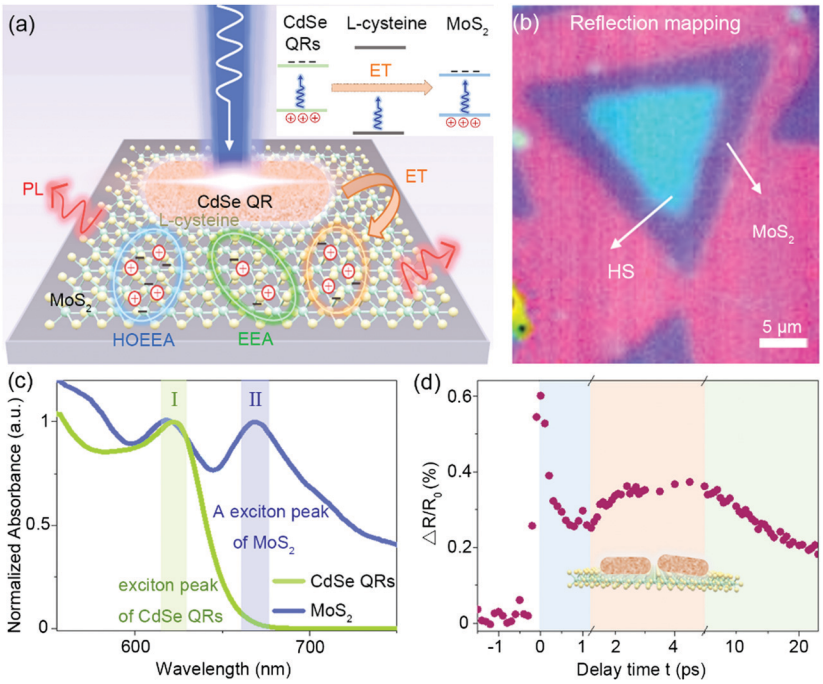

Fig. 1 Schematic of the structure and spectra of the MoS_2/CdSe QR heterostructure. (a) Illustration of the heterostructure, where the CdSe QRs are placed on a MoS_2 monolayer. The orange, blue, and green circles represent energy transfer, EEA, and HOEEA processes, respectively. Inset is the band structure illustration of the MoS_2 monolayer, CdSe QR, and L-cysteine molecule. The orange arrow represents energy transfer. (b) Reflection mapping of the heterostructure. The homogeneous light blue area indicates the near-uniform distribution of CdSe QRs on the MoS_2 monolayer (purple). (c) Normalized absorption spectra of CdSe QRs (green) and the MoS_2 monolayer (blue). (d) Time-resolved differential reflection signal of the heterostructure, with the blue, orange and green areas representing the dominating HOEEA, energy transfer, and EEA processes. The pump light is fixed on 400 nm with a fluence of 14.4 μJ cm^{-2} and the probe light is fixed on 675 nm with the fluence of 0.58 μJ cm^{-2}.

is shown in Fig. S13, ESI†). The corresponding absorption spectra of CdSe QRs and MoS_2 monolayer are shown in Fig. 1(c). The signals of the CdSe QRs and MoS_2 monolayer are normalized by the intensity of peak I and II, respectively, to highlight the peak positions. Peak I, located at 620 nm, is the exciton peak of CdSe QRs and peak II, at 670 nm, is the A exciton of the MoS_2 monolayer, which provides wavelength information for pump–probe measurements. In the time-resolved differential reflection measurement (Fig. 1(d)), the signal of MoS_2 in the heterostructure displays three different decay processes corresponding to the exciton relaxation by HOEEA, energy transfer, and EEA, as seen in Fig. 1(a). The unique exciton decay of the MoS_2 acceptor in the heterostructure contributes to PL enhancement, which will be discussed later and is shown in Fig. 3.

PL measurements were employed to study the light-emitting properties of the heterostructure, with the PL spectra of the pristine MoS_2 monolayer and CdSe QRs for comparison. As shown in Fig. 2(a), peak I and II are located at 624 nm and 672 nm and are attributed to the PL peaks of the MoS_2 monolayer and CdSe QRs, respectively. After forming the MoS_2/CdSe QR heterostructure, the PL peak I has approximately 50% attenuation and the attenuation of peak II increases to about 230%. In the presence of the CdSe layer, the amount of excitation light that reaches MoS_2 is reduced and the PL of MoS_2 should be weakened, which is contrary to the experimental results. This implies that the different amount of excitation light is not the reason for the enhanced PL of MoS_2. The typical PL spectrum of energy transfer is shown in Fig. 2(a) with the donor signal decreasing and the acceptor signal increasing. This is the direct evidence for energy transfer from the CdSe QRs to the MoS_2 monolayer.[23] If the charge transfer dominates, the PL signals of the donor and acceptor should both decrease.[24,25] Thus, it is evident that energy transfer is the dominating interaction in the heterostructure. Since the PL intensity of CdSe QRs is much larger than that of MoS_2, the 50% decrease in the energy of CdSe QRs is large enough to result in a 230% energy enhancement of MoS_2. In order to further explore the light-emitting properties of the heterostructure, the excitation fluence was increased from 1.4 μJ cm^{-2} to 21.6 μJ cm^{-2} (Fig. S1, ESI†). On one hand, the PL peaks I and II of the heterostructure grow with similar trend, as shown in Fig. 2(b), which suggests that the energy transfer from CdSe to MoS_2 has modulated the light emission of the heterostructure. On the other hand, the MoS_2 in the heterostructure is further enhanced as the excitation fluence increases, and it reaches 500% when the pump fluence increases to 21.6 μJ cm^{-2} (Fig. 2(c)). Since the rate of the nonradiative energy transfer is related to distance, spectral overlap, and the relative polarization between the donor and acceptor, the energy transfer induced enhancement of MoS_2 in the heterostructure should not be altered by a change in the pump fluence, implying that there is another mechanism that improves the radiative emission of MoS_2.

PL emission is decided by the exciton population (N) and the radiative and nonradiative channels of the exciton relaxation process. In order to explore the mechanism of enhanced PL, theoretical analysis of the exciton relaxation dynamics of the heterostructure from the aspect of MoS_2 is employed.

In a pristine MoS_2 monolayer, the relaxation process, including exciton recombination, EEA, and HOEEA, can be expressed as[26–28]

$$\frac{dN}{dt} = -k_{ER}N - k_{EEA}N^2 - k_{HOEEA}N^4 - \dots \quad (1)$$

where k_{ER}, k_{EEA}, and k_{HOEEA} represent the rate of exciton recombination, EEA, and HOEEA processes. When the value of N is large, higher-order terms dominate the relaxation process and the role of lower-order terms is less important. As N decreases, lower-order terms appear to guide the exciton relaxation and the influence of higher-order terms is gradually diminished.

When energy transfer plays a role in exciton relaxation, the relaxation equation should be modified. In the energy transfer process, the exciton population of the donor (N_D) can be simplified to $N_D = N_{D_1}e^{-k_{ET}t}$, where N_{D_1} is a constant, and k_{ET} represents the energy transfer rate. When the donor consumes $\Delta N_{D(ET)}$ in the energy transfer process, the acceptor acquires excitons $\Delta N_A = \Delta N_{D(ET)}$. Thus, the acquired exciton population of the acceptor

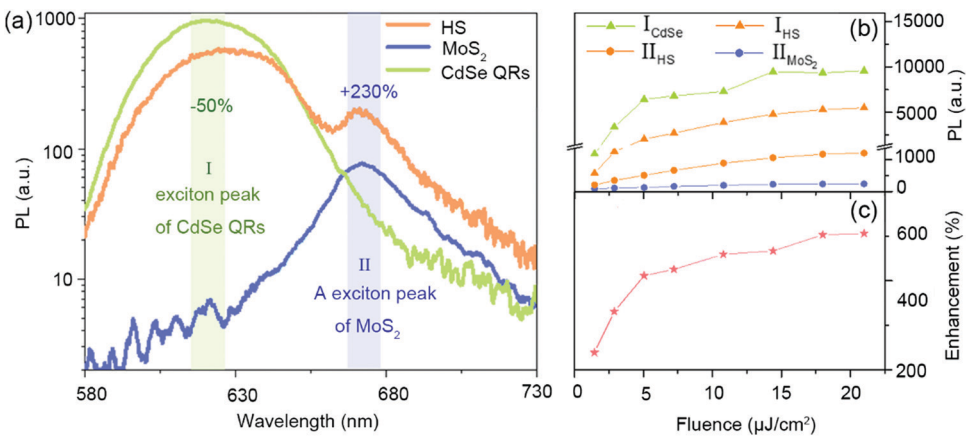

Fig. 2 (a) PL spectra of heterostructure (orange), pristine MoS_2 monolayer (blue), and CdSe QRs (green). (b) PL intensity of all of the heterostructure, MoS_2, and CdSe QRs. (c) PL enhancement of MoS_2 as a function of incident fluence. Defining II_{HS}/II_{MoS_2} as PL enhancement.

(N_A) can be written as $\frac{dN_A}{dt} = k_{ET}N_D = k_{ET}N_{D_1}e^{-k_{ET}t}$, indicating that for the acceptor, there is an "exciton re-excitation" process (Section S7, ESI†). Based on the above analysis, the exciton population of the acceptor can be expressed as:

$$\frac{dN_A}{dt} = k_{ET}N_{D_1}e^{-k_{ET}t} - k_{ER}N_A - k_{EEA}N_A{}^2 - k_{HOEEA}N_A{}^4 - \ldots \quad (2)$$

To experimentally reveal the exciton relaxation dynamics from the standpoint of the acceptor, femtosecond pump–probe measurements were performed. The time-resolved differential reflection signal can be expressed as $\Delta R/R_0 = (R - R_0)/R_0$, where R and R_0 correspond to the reflective signal with and without the sample, respectively. It refers to the relative reflective difference of the probe laser induced by the pump laser, representing the variation in exciton population (N) (Fig. S6, ESI†). The relaxation dynamics of the heterostructure and pristine MoS_2 monolayer are presented in Fig. 3(a), with Fig. 3(b)–(d) illustrating the corresponding dynamics with the same background color. The signal $\Delta R/R_0$ was measured at a pump fluence of 14.4 μJ cm^{-2} at the wavelength of 400 nm, and the probe wavelength was fixed at 675 nm with a fluence of 0.58 μJ cm^{-2}, which corresponds to the energy of the A exciton of MoS_2. The $\Delta R/R_0$ signal of CdSe QRs is negligible because the absorption of CdSe QRs at 675 nm can be ignored (Fig. 1(c)).

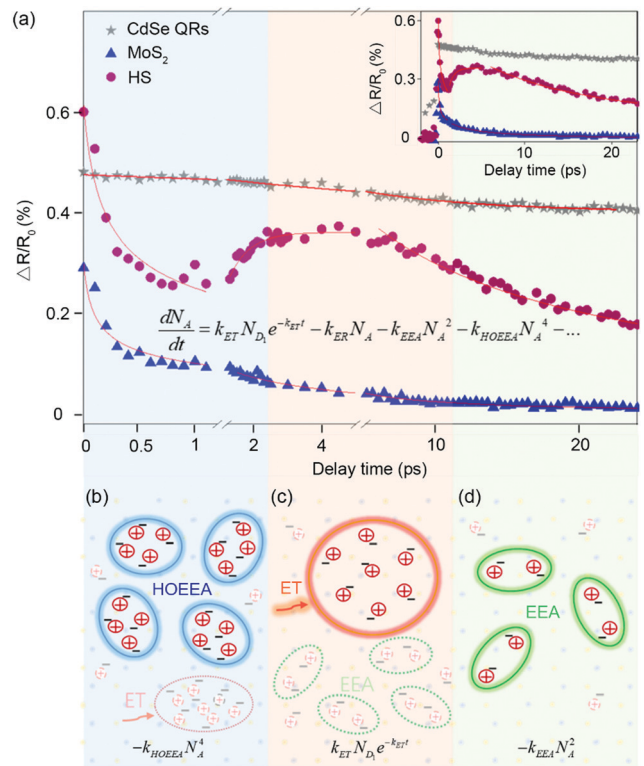

Fig. 3 Temporal evolution of the exciton population. (a) Time-resolved differential reflection signal of the heterostructure (red dots), pristine MoS_2 monolayer (blue triangles), and pure CdSe QRs (gray starts) with a pump laser of 400 nm and probe laser of 675 nm. Inset is the signal with a linear time scale. The exciton relaxation process of the heterostructure can be divided into four parts: (b) HOEEA, (c) energy transfer, and (d) EEA dominating. The blue, orange, and green circles suggest that the excitons are undergoing HOEEA, energy transfer, and EEA processes. The shining solid circles and dotted circles imply that there are dominant and minor relaxation processes in the corresponding time periods, respectively.

The exciton relaxation dynamics of the pristine MoS_2 monolayer and heterostructure were analyzed, as shown in Fig. 3(a). It should be noted that in this study the effects of coherent phonons were excluded (Section S7, ESI†). For the pristine MoS_2 monolayer, it can be clearly observed that the exciton relaxation consists of two different processes, as displayed in eqn (1). In the first 1 ps, high order interactions among excitons, HOEEA, dominates the decay process and is expressed as $\frac{dN}{dt} = -k_{HOEEA}N^4$. As time goes by, the interactions of HOEEA diminish and are followed by EEA, with the kinetic equation: $\frac{dN}{dt} = -k_{EEA}N^2$. The value of k_{EEA} is obtained as $k_{EEA} = 0.417 \pm 0.050$ cm^2 s^{-1}, which is in agreement with that obtained in previous studies,[29,30] verifying the reliability of these experimental methods and the analytical approaches used in this work.

As for the heterostructure, the exciton relaxation can be described by eqn (2). However, the modified model in eqn (2) has four free parameters, which hinder the analysis of the experimental data. Luckily, the four relaxation processes dominate at different time scales. Thus, it is reasonable to divide the whole relaxation process into four parts, with each part having one free parameter. In the beginning, excitons quickly decay to the band edge level after they are pumped to high energy levels. Under this condition, the "crowded" excitons tend to undergo high order interactions, HOEEA, contributing to the rapid descent of N_A (Fig. 3(b)). About 1 ps later, the effect of HOEEA is rapidly weakened, and the role of energy transfer emerges, leading to an overall enhancement of N_A, as shown in Fig. 3(c). The corresponding dominant relaxation equation is expressed as $\frac{dN}{dt} = k_{ET}N_{D_1}e^{-k_{ET}t}$, with the energy transfer rate as $k_{ET} = 17.41 \pm 0.13$ ns^{-1}. When $t > 5$ ps, the effect of energy transfer is gradually diminished, and EEA starts to dominate the relaxation process and N_A decreases again (Fig. 3(d)).

Compared to the signal of the pristine MoS_2 monolayer, the most obvious difference is the increase in N_A after the HOEEA process, which is the direct evidence of energy transfer. It should be mentioned that this is the first direct observation of the increase in N_A induced by energy transfer, benefitting from the ultra-short probe time step length of 100 fs. In the heterostructure, energy is transferred from donor CdSe QRs to acceptor MoS_2 in the form of additional excitons. These excitons are equivalent to an extra "source" for PL, which lays the foundation for the enhanced PL of the heterostructure. However, if the following nonradiative interaction (EEA) in the MoS_2 acceptor is active, there still would be a large portion of excitons decayed in a nonradiative way, impeding luminescence of the material. In this study, the EEA of the heterostructure is effectively suppressed, with $k_{EEA(HS)}/k_{EEA(MoS_2)} \approx 0.091$. The existence of CdSe QRs affects the dielectric environment with a larger refractive index than air. Additionally, the Coulomb

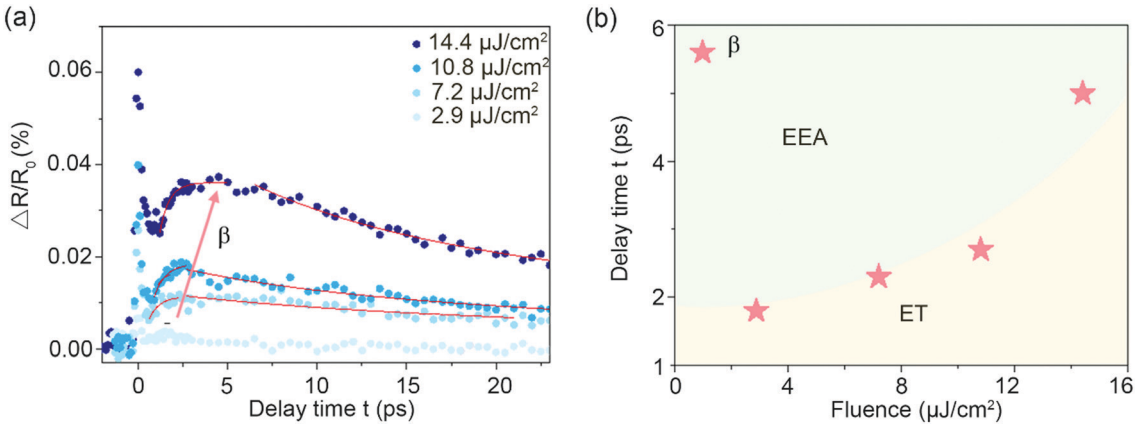

Fig. 4 (a) Time-resolved transient differential reflection spectra of the heterostructure as a function of pump fluence. (b) The appearance time of point β as a function of pump fluence. The area with a yellow background indicates that energy transfer dominates exciton relaxation, while the area with a green background implies that exciton relaxation is dominated by EEA.

interactions in MoS_2 can be reduced by leaking into the surrounding environment,[31] resulting in a smaller $k_{EEA(HS)}$ compared to $k_{EEA(MoS_2)}$ (Fig. S7, ESI†). Alternatively, surface modification by CdSe QRs can effectively suppress the EEA process to reduce the nonradiative loss. The existence of CdSe QR-induced energy transfer optimizes the dielectric environment, contributing to the enhanced PL of the heterostructure.

In order to further optimize the PL emission of the heterostructure, the contribution of energy transfer and EEA to the exciton relaxation process was investigated. When the contribution of energy transfer becomes larger, more excitons are provided for emission. When the contribution of EEA gets higher, more excitons decay through a nonradiative pathway. Through tuning the fluence of the pump laser, the effect of energy transfer and EEA on exciton relaxation can be efficiently modulated. In Fig. 4(a), the modulation is reflected by the emerging time of inflection point β between the two processes. At point β, the effect of energy transfer diminishes and EEA starts to dominate the exciton relaxation dynamics. By increasing the pump fluence from 2.9 μJ cm^{-2} to 14.4 μJ cm^{-2}, the appearance time of point β is increased, where the effect of energy transfer on exciton relaxation is stronger in comparison to that of EEA, as shown in Fig. 4(b). As energy transfer is independent of the excitation fluence, the variation in point β indicates a change to EEA. When the pump fluence is relatively low, EEA can be mediated by some defect trapping processes.[32] In this situation, k_{EEA} keeps reducing until all of the defect states become occupied when the pump fluence is increasing. Thus, in the heterostructure, EEA shows a decreasing trend as the pump fluence increases (Fig. S11, ESI†), resulting in an increase in exciton due to the effects of energy transfer compared to EEA, ultimately improving PL under high fluence excitation.

Conclusions

In conclusion, the mechanism of PL enhancement from the standpoint of the acceptor in the MoS_2/CdSe QR heterostructure was studied using the femtosecond pump–probe technique. Energy transfer induced "extra excitons" and the CdSe QRs induced the suppression of nonradiative EEA, which resulted in the PL enhancement of the heterostructure. It is the first direct observation of an increase in N_A induced by energy transfer using the time-resolved differential reflection signal. An energy transfer term was added to modify the exciton relaxation dynamics equation to systematically investigate the exciton relaxation dynamics from the standpoint of the acceptor, which has far-reaching significance for more sophisticated multi-physical processes. Our work advances the basic comprehension of the exciton dynamics of the energy acceptor and paves the way for developments of new high-performance optical conversion, on-chip light emission, and light-sensing devices.

Methods

Sample fabrication

The MoS_2 monolayer was grown using the chemical vapor deposition (CVD) method at 850 °C, with MoO_3 and pristine sulphur as the reaction materials. The silicon substrate was covered by a 540 nm SiO_2 film.[33] CdSe QRs with a diameter of 3.75 ± 0.47 nm and an aspect ratio of 4.82 ± 0.81 were synthesized in trioctylphosphine oxide, following the thermal injection technique (Fig. S12, ESI†). Subsequent ligand exchange allowed QRs to be coated with cysteine without geometric destruction.[34,35] To avoid bubbles caused by the strain effect, the heterostructure was fabricated by spin-coating a CdSe QR solution onto the MoS_2 monolayer, followed by water evaporation in a nitrogen cabinet at room temperature.

Optical measurements

Reflection mapping and absorption spectra were measured using a hyperspectral imaging system (Cytoviva HIS V3) and detected using a spectrometer (Horiba IHR550) with a 100× objective lens (Olympus MPlanFL N, NA = 0.9). The absorption spectra were recorded from the relative reflection change of sample compared with the substrate. Raman spectra were recorded using a home-built optical system and detected using a spectrometer (Horiba IHR550) with a 50× objective lens (Olympus LUCPlanFL N, NA = 0.5) and a 2400 g mm^{-1} grating for high resolution.

Pump–probe and PL measurements were conducted using a home-build optical system. A detailed description can be referred to in previous study.[36] Femtosecond pulse with a repetition rate of 80 MHz and pulse duration of ~84 fs was produced using a mode-locked oscillator (Tsunami 3941C-25XP). The output 800 nm pulse was split into two parts. One was focused on a BBO crystal to generate the 400 nm pump light, which was modulated using a chopper with 1500 MHz and the other one passed through a photonic fiber crystal (Newport SCG-800) to produce super-continuum white light. The time delay between the pump and probe pulse was controlled by a steeper linear stage (Newport M-ILS150PP) and limited by a mode-locked oscillator. Only two pump wavelengths were available: 400 nm and 800 nm. The pump and probe lights were focused by a 40× objective lens (Olympus LUCPlanFL N, NA = 0.6). The reflected probe signal was focused on a high-sensitivity photomultiplier (Thorlabs PMM02). The PL spectra were measured using a spectrometer (Princeton Action SP2500) with a 600 mm^{-1} grating. As the PL and pump–probe collection corresponded to the coupling of optical elements (lens, reflection mirror, filter, fibre, *etc.*) and the spectrograph, all of the measurement parameters remain unchanged to avoid the collection efficiently changing.

Author contributions

Z. F. and Y. L. conceived the idea and designed the research. Y. L. and H. S. performed the pump–probe and PL measurements. Y. L. and X. G. fabricated the samples. Y. L. and B. L. performed the reflection measurement. Y. L., P. Q., and H. Z. performed the theoretical simulation. Y. L., Z. F., P. Q., and H. Z. revised the manuscript. All authors discussed the results and commented on the manuscript.

Conflicts of interest

There are no conflicts to declare.

Acknowledgements

This work is supported by the National Key Research and Development Program of China (grant no. 2019YFA0210203, 2017YFA0205700 and 2017YFA0206000), National Science Foundation of China (grant no. 11674012, 61521004, 21790364, 61422501 and 11374023), Beijing Natural Science Foundation (grant no. Z180011 and L140007), and Foundation for the Author of National Excellent Doctoral Dissertation of China (grant no. 201420), National Program for Support of Top-notch Young Professionals (grant no. W02070003).

References

1 J. Shi, M. H. Lin, I. T. Chen, N. Mohammadi Estakhri, X. Q. Zhang, Y. Wang, H. Y. Chen, C. A. Chen, C. K. Shih, A. Alu, X. Li, Y. H. Lee and S. Gwo, *Nat. Commun.*, 2017, **8**, 35.
2 X. Liu and J. Qiu, *Chem. Soc. Rev.*, 2015, **44**, 8714–8746.
3 A. Henning, V. K. Sangwan, H. Bergeron, I. Balla, Z. Sun, M. C. Hersam and L. J. Lauhon, *ACS Appl. Mater. Interfaces*, 2018, **10**, 16760–16767.
4 Y. Tan, L. Ma, Z. Gao, M. Chen and F. Chen, *Nano Lett.*, 2017, **17**, 2621–2626.
5 X. Shi, K. Ueno, T. Oshikiri, Q. Sun, K. Sasaki and H. Misawa, *Nat. Nanotechnol.*, 2018, **13**, 953–958.
6 B. Hunt, J. Sanchez-Yamagishi, A. Young, M. Yankowitz, B. J. LeRoy, K. Watanabe, T. Taniguchi, P. Moon, M. Koshino and P. Jarillo-Herrero, *Science*, 2013, **340**, 1427–1430.
7 L. Pi, L. Li, K. Liu, Q. Zhang, H. Li and T. Zhai, *Adv. Funct. Mater.*, 2019, 1904932, DOI: 10.1002/adfm.201904932.
8 N. R. Glavin, R. Rao, V. Varshney, E. Bianco, A. Apte, A. Roy, E. Ringe and P. M. Ajayan, *Adv. Mater.*, 2019, e1904302, DOI: 10.1002/adma.201904302.
9 A. Raja, A. Montoya Castillo, J. Zultak, X. X. Zhang, Z. Ye, C. Roquelet, D. A. Chenet, A. M. van der Zande, P. Huang, S. Jockusch, J. Hone, D. R. Reichman, L. E. Brus and T. F. Heinz, *Nano Lett.*, 2016, **16**, 2328–2333.
10 L. Wu, Y. Chen, H. Zhou and H. Zhu, *ACS Nano*, 2019, **13**, 2341–2348.
11 D. Katz, T. Wizansky, O. Millo, E. Rothenberg, T. Mokari and U. Banin, *Phys. Rev. Lett.*, 2002, **89**, 086801.
12 B. Peng, Z. Li, E. Mutlugun, P. L. Hernandez Martinez, D. Li, Q. Zhang, Y. Gao, H. V. Demir and Q. Xiong, *Nanoscale*, 2014, **6**, 5592–5598.
13 D. O. Sigle, L. Zhang, S. Ithurria, B. Dubertret and J. J. Baumberg, *J. Phys. Chem. Lett.*, 2015, **6**, 1099–1103.
14 D. Prasai, A. R. Klots, A. K. Newaz, J. S. Niezgoda, N. J. Orfield, C. A. Escobar, A. Wynn, A. Efimov, G. K. Jennings, S. J. Rosenthal and K. I. Bolotin, *Nano Lett.*, 2015, **15**, 4374–4380.
15 F. Prins, A. J. Goodman and W. A. Tisdale, *Nano Lett.*, 2014, **14**, 6087–6091.
16 S. Sampat, T. Guo, K. Zhang, J. A. Robinson, Y. Ghosh, K. P. Acharya, H. Htoon, J. A. Hollingsworth, Y. N. Gartstein and A. V. Malko, *ACS Photonics*, 2016, **3**, 708–715.
17 N. Taghipour, P. L. Hernandez Martinez, A. Ozden, M. Olutas, D. Dede, K. Gungor, O. Erdem, N. K. Perkgoz and H. V. Demir, *ACS Nano*, 2018, **12**, 8547–8554.
18 N. Kumar, Q. Cui, F. Ceballos, D. He, Y. Wang and H. Zhao, *Phys. Rev. B: Condens. Matter Mater. Phys.*, 2014, **89**, 125427.
19 M. Beerbom, R. Gargagliano and R. Schlaf, *Langmuir*, 2005, **21**, 3551–3558.
20 H. Shan, Y. Yu, X. Wang, Y. Luo, S. Zu, B. Du, T. Han, B. Li, Y. Li, J. Wu, F. Lin, K. Shi, B. K. Tay, Z. Liu, X. Zhu and Z. Fang, *Light: Sci. Appl.*, 2019, **8**, 9.
21 J. Hu, L. Wang, L.-S. Li, W. Yang and A. P. Alivisatos, *J. Phys. Chem. B*, 2002, **106**, 2447–2452.
22 X. Xu, S. Giménez, I. Mora-Seró, A. Abate, J. Bisquert and G. Xu, *Mater. Chem. Phys.*, 2010, **124**, 709–712.
23 J. Gu, X. Liu, E.-C. Lin, Y.-H. Lee, S. R. Forrest and V. M. Menon, *ACS Photonics*, 2017, **5**, 100–104.
24 X. Hong, J. Kim, S. F. Shi, Y. Zhang, C. Jin, Y. Sun, S. Tongay, J. Wu, Y. Zhang and F. Wang, *Nat. Nanotechnol.*, 2014, **9**, 682.

25 S. Kaniyankandy, S. Rawalekar and H. N. Ghosh, *J. Phys. Chem. C*, 2012, **116**, 16271–16275.
26 D. Sun, Y. Rao, G. A. Reider, G. Chen, Y. You, L. Brezin, A. R. Harutyunyan and T. F. Heinz, *Nano Lett.*, 2014, **14**, 5625–5629.
27 H. Shan, Y. Yu, R. Zhang, R. Cheng, D. Zhang, Y. Luo, X. Wang, B. Li, S. Zu, F. Lin, Z. Liu, K. Chang and Z. Fang, *Mater. Today*, 2019, **24**, 10–16.
28 S. Hao, M. Z. Bellus, D. He, Y. Wang and H. Zhao, *Nanoscale Horiz.*, 2020, **5**, 139–143.
29 Y. Yu, Y. Yu, C. Xu, A. Barrette, K. Gundogdu and L. Cao, *Phys. Rev. B: Condens. Matter Mater. Phys.*, 2016, **93**, 201111.
30 S. Mouri, Y. Miyauchi, M. Toh, W. Zhao, G. Eda and K. Matsuda, *Phys. Rev. B: Condens. Matter Mater. Phys.*, 2014, **90**, 155449.
31 D. Jena and A. Konar, *Phys. Rev. Lett.*, 2007, **98**, 136805.
32 B. Liu, Y. Meng, X. Ruan, F. Wang, W. Liu, F. Song, X. Wang, J. Wu, L. He, R. Zhang and Y. Xu, *Nanoscale*, 2017, **9**, 18546–18551.
33 S. Najmaei, Z. Liu, W. Zhou, X. Zou, G. Shi, S. Lei, B. I. Yakobson, J. C. Idrobo, P. M. Ajayan and J. Lou, *Nat. Mater.*, 2013, **12**, 754–759.
34 Z. A. Peng and X. Peng, *J. Am. Chem. Soc.*, 2001, **123**, 1389–1395.
35 X. Gao, X. Zhang, K. Deng, B. Han, L. Zhao, M. Wu, L. Shi, J. Lv and Z. Tang, *J. Am. Chem. Soc.*, 2017, **139**, 8734–8739.
36 Y. Yu, Z. Ji, S. Zu, B. Du, Y. Kang, Z. Li, Z. Zhou, K. Shi and Z. Fang, *Adv. Funct. Mater.*, 2016, **26**, 6394–6401.